RSC Advances

ROYAL SOCIETY OF CHEMISTRY

www.rsc.org/advances

RSC Advances

RSCPublishing

ARTICLE

Raspberry-like morphology of polyvinyl chloride-zinc oxide nanoparticles induced by surface interaction for nanoporous foam

Cite this: DOI: 10.1039/x0xx00000x

Received 00th January 2012,
Accepted 00th January 2012

DOI: 10.1039/x0xx00000x

www.rsc.org/

Tingting Ren [a], Jie Wang [a], Jinfeng Yuan [a], Mingwang Pan [a,*], Gang Liu [a], Guanglin Zhang [a], Gan-Ji Zhong [b,*], Zhong-Ming Li [b]

This work presents a facile approach to synthesize P(VC-co-AAEM) (vinyl chloride copolymerized acetoacetoxyethyl methacrylate)/zinc oxide (ZnO) nanocomposite particles with raspberry-like shape by nano-coating technique. It is proved that the interactions between β-diketone groups embedded in AAEM and ZnO precursors are crucial to forming raspberry-like morphology, as such, the content of AAEM has a significant effect on the nucleation and growth of ZnO nanocrystals on the P(VC-co-AAEM) beads. SEM analysis demonstrated that ZnO nanocrystals were deposited on the surface of template nanoparticles as small clusters with different sizes and quantity, depending on the reaction parameters. X-ray diffraction of the P(VC-co-AAEM)/ZnO nanocomposite particles revealed that the addition of functionalized PVC beads lowered the formation of ZnO nanocrystals due to constrained effect of ZnO-AAEM interaction on the mobility of ZnO precusors. Additionally, such PVC/ZnO composite particles were found to have excellent foamability of nanometer-sized pores, which could have various potential applications in sound insulation and thermal insulation.

Introduction

Today the chemists are interested in tailoring various shapes of complex hybrid systems with perfect performance at different components, size scales, and functionalities using cross-cutting approaches, where molecular engineering and intelligent processing are synergistically coupled. Hybrid materials with organic–inorganic character not only represent a new field of basic research, but also offer prospects for many new applications due to their remarkable new properties and multifunctional nature.[1] Clearly, the properties of these hybrids aren't only the sum of the individual contributions of two phases where the interfaces always play a most predominant role. Based on the nature of the interface, these materials were grossly divided into two distinct classes.[2] In *class I* materials, organic and inorganic components are constituted and only weak bonds (hydrogen, van der Waals or ionic bonds) give the cohesion to the whole structure. In *class II* materials, the two phases are linked together through strong chemical covalent bonds. Currently, most of the hybrid materials that have already entered the market are synthesized and processed by using conventional chemistry routes developed in the eighties.[3] These processes are based on: a) the copolymerization of functional organosilanes, macromonomers, and metal alkoxides, b) the encapsulation of organic components via sol–gel derived silica or metallic oxides, c) the organic functionalization of nanofillers, nanoclays or other compounds with lamellar structures, *etc*. Wu group[4-6] utilized a variety of non-covalent interaction between organic and inorganic components to get a series of composite microspheres with raspberry-like, core-shell and multi-layer shapes by templating polymer particles or inorganic nanoparticles. Liu[7,8] synthesized snowman-like or raspberry-like polymer-silica asymmetric particles by combination of hydrolytic condensation process with γ-ray radiation initiated seeded emulsion polymerization or by soap-free emulsion polymerization and sol–gel process. Yang[9] recently described the deposition of Fe_3O_4 inorganic substance on polymer with Janus cage shape through an emulsion interfacial self-organized sol−gel process followed by a polymer grafting onto the interior surface containing a vinyl group.

Nowadays, nano-coating techniques result in the formation of novel inorganic–organic functional hybrid materials with tailored performances that depend on the combination of components employed in the fabrication process. The major templates used for preparation of hybrid materials can be produced at present with monodispersed colloid particles or controlled morphology (such as membrane pore structure). For the synthesis of inorganic particles, the most common method is based on solution phase. This method has been used to synthesize nanoparticles of II-VI compounds (*e.g.*, CdS,

PbS),[10,11] III-V compounds (GaAs)[12] and a wide range of metal oxides including TiO_2,[13] ZnO,[14] Fe_2O_3,[15] and PbO,[16] Fe_3O_4.[17]

Nano-ZnO, as one of the multifunctional inorganic nanoparticles, has drawn increasing attention in recent years due to its many significant physical and chemical properties, such as chemical stability,[18] low dielectric constant,[19] high transmittance,[20] high catalysis activity,[21,22] effective antibacterial and bactericidal action,[23,24] UV-screening[25,26] and infrared absorption.[27] Therefore, nano-ZnO can be potentially applied to UV-shielding material,[26,26] catalyst,[21,22] antibacterial materials,[23,24] sensor,[19] solar cells[28,29] and so forth. Tang[30] reported the preparation of styrene polymer/ZnO nanocomposite latex via miniemulsion polymerization and its antibacterial property. Liufu[31] demonstrated the thermal property and degradation mechanism of polyacrylate/ZnO nanocomposites. He[32] has successfully prepared polyaniline/nano-ZnO composites via a novel Pickering emulsion route. Intriguingly, Agrawal[33] reported on the preparation of polystyrene-ZnO composite particles with controlled morphology. First, such particles with raspberry-like morphology can find application as a carrier of ZnO nanoparticles into suitable polymer matrices to obtain ZnO nanoparticles with better dispersion. For example, Stamm[34] has successfully mixed the raspberry-shaped polystyrene/ZnO composite particles into poly(ethyl methacrylate) (PEMA) matrix, in which the PS/ZnO domains showed a homogenous distribution. A significant enhancement in the thermal stability and mechanical properties of the PEMA matrix has been discovered.

Moreover, organic–organic asymmetric particles with adjustable shape and unique physicochemical properties have been prepared by our group.[35,36] In the present study, we report on a novel and facile approach to *in situ* preparation of polyvinyl chloride/ZnO nanocomposite particles with raspberry-like shape. The study interest arises from their interesting morphology and unique combination of advantages. And this system provides flexibilities in size, content and morphological variation of ZnO. Further, as a main motivation of this research, as-prepared raspberry-like PVC/ZnO particles also have great application in foam field. ZnO as an azodicarbonamide (ADC) accelerating agent can decrease the decomposing temperature of ADC which was the most popular chemical foaming agent for PVC foam.[37,38] And it is well known that PVC products have many outstanding advantages (low cost, flexible formulation, excellent chemical resistance, fire retardant performance, and high mechanical strength) and extensive applications. A small amount of well-dispersed nanoparticles in the polymer may serve as nucleation sites to facilitate the bubble nucleation process. Thereby, this research attempts to turn the dissymmetrical PVC/ZnO composite particles into foam material to extend their application field.

Experimental Section

Materials

Vinyl chloride (VC, above 99.99 wt% purity) was kindly provided by the Tianjin Chemical Plant (Tianjin, China). Potassium persulfate (KPS, above 99.5 wt%, China Medicine Group Chemical Reagent Co., Ltd.) and acetoacetoxyethyl methacrylate (AAEM, Beijing Baiyuan Chemical Co., Ltd., Beijing, China) monomer was used without further purification. Zinc acetate dihydrate ($Zn(Ac)_2\ 2H_2O$, 99.0%), sodium hydroxide (NaOH, analytical grade), dimethyl sulfoxide (DMSO, 99.5%), azodicarbonamide (ADC, commercially pure), and isopropyl alcohol (IPA, 99.7%) were all obtained from the Tianjin Chemical Reagent Co., Ltd. (Tianjin, China). Tetrahydrofuran (THF, 99.0%) was purchased from the Tianjin Shengmiao Fine Chemical Co. Ltd. (Tianjin, China), and Zinc oxide (ZnO, 99.0%) was obtained from the Tianjin Huadong Reagent Factory (Tianjin, China). Above chemical reagent was used as received. Distilled water was employed as the polymerization medium.

Synthesis of P(VC-co-AAEM) Particles

For clear understanding, a desired fabrication route to foaming PVC sheet is demonstrated in Scheme 1. Functionalized P(VC-co-AAEM) (VC copolymerizing AAEM) template particles were synthesized by surfactant-free emulsion polymerization as shown in Scheme 1a.

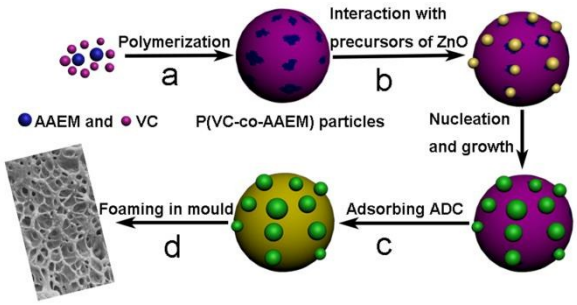

Scheme 1 Schematic representation of the steps involved in the fabrication of P(VC-co-AAEM) /ZnO composite particles and foaming: (a) preparing functionalized P(VC-co-AAEM) particles, (b) fabrication of P(VC-co-AAEM)/ZnO nanocomposite particles, (c) absorbing ADC, (d) foaming in mould.

Table 1 summarizes polymerization recipe used in the preparation of template particles. First of all, a given amount of deionized water, KPS (1.2 wt% of monomer), and AAEM were introduced into a 2 L autoclave at room temperature. Then, the autoclave was vacuumed and charged with nitrogen repeatedly three times to remove O_2 fully. The reaction mixture was stirred for 20 min at a speed of 300 rpm. Then, VC monomer was added in one batch. The mixture was continuously stirred to mix the VC and AAEM monomers uniformly. After 20 min, the mixture was heated up to 55 ℃ quickly to initiate this polymerization. When the pressure in the reaction dropped to

0.25 MPa, the reaction system was cooled down to room temperature promptly, and then vacuumed to remove the unreacted VC from P(VC-co-AAEM) latex. The obtained P(VC-co-AAEM) latex was filtered and sampled for measurement of solid content and morphology observation.

Table 1 Polymerization recipe for P(VC-co-AAEM) latex particles used in this work

Sample no.	VC (g)	AAEM (wt% VC)	Water (g)	D_p* (nm)	PDI**
a	60	0	600	359.4	0.048
b	60	10	600	381.6	0.039
c	60	15	600	368.4	0.030
d	60	20	600	346.5	0.059

* Mean diameter of P(VC-co-AAEM) particles determined by dynamic laser scattering technique

** PDI indicating polydispersity index of particle diameter

Synthesis of ZnO nanocrystals and P(VC-co-AAEM)/ZnO Nanocomposite Particles

Solution phase method has been widely used for the synthesis of crystalline nanoparticles. Typically, the synthesis of metal oxide nanoparticles involves the reaction of a metal salt with hydroxide ion.[39] In this study, we prepared ZnO from $Zn(Ac)_2$ in IPA with the addition of NaOH aqueous solution.[40] The overall nucleation reaction can be written as:

$$ZnX_2 + 2NaOH \rightarrow ZnO + 2NaX + H_2O$$

First, a given amount of $Zn(Ac)_2\ 2H_2O$ salt was added to IPA solution (from set 1 in Table 2) in a three-necked round-bottom flask equipped with a condenser, a Teflon blade mechanical stirrer and a thermometer. After stirring at 20 ℃ for 20 min, the well mixture was heated to 55 ℃ rapidly and stirred for another 1 h. At this stage, for the preparation of P(VC-co-AAEM)/ZnO composite particles (see Scheme 1b), 5.0 g of latex (containing 0.45 g of P(VC-co-AAEM) solid particles) were added to the reaction mixture and kept stirring for 20 min. After that, the reaction mixture was cooled to 20 ℃ followed by adding a set concentration of NaOH aqueous solution at a speed of 0.25 mL min^{-1}. Afterward, the reaction mixture was kept at 55 ℃ for a couple of hours. Finally, the solution was cooled to 20 ℃, and the solvent was removed via rotary evaporation at 50 ℃. The obtained ZnO nanocrystals or P(VC-co-AAEM)/ZnO nanocomposite was washed three times with distilled water following centrifugation, and dried in a vacuum oven at 40 ℃.

Table 2 Variation in reaction parameters during preparation of ZnO nanocrystals and P(VC-co-AAEM)/ZnO composite particles

Reaction set	Concentration NaOH (M)	Volume NaOH (mL)	Concentration $Zn(Ac)_2{\cdot}2H_2O$ (mM)	Volume C_3H_7OH (mL)	Latex solid particles[a] (g)
1	0.2[b], 0.5, 1.0	2	2.0	80	0.45
2	0.2	4	2.0	160	0.45
3	0.2	6	2.0	240	0.45
4	0.2	8	2.0	320	0.45
5	0.2	10	2.0	400	0.45

[a] During the synthesis of P(VC-co-AAEM)/ZnO composite particles, P(VC-co-AAEM) containing 10wt%AAEM was chosen as the template.

[b] During the synthesis of ZnO nanocrystals, other reaction parameters are the same except template particles.

Preparation of P(VC-co-AAEM)/ZnO Nanocomposite Foam Material

The preparation of P(VC-co-AAEM)/ZnO composite foam consists of two experimental parts, as shown in Scheme 1 c and d. First, a right amount of ADC (dissolved in DMSO) was added in the above P(VC-co-AAEM)/ZnO dispersion. The mixture was vigorously stirred for 4 h. Afterwards, the P(VC-co-AAEM)/ZnO particles adsorbed with ADC on the surface were achieved after centrifugation and rotary evaporation, then thoroughly dried by vacuum freeze-drying machine. The second part concentrated on preparation of PVC foams. As-prepared powder dispersed with a heat stabilizer was put in a mould (40*15*2 mm^3). Then the mould was placed on a flat vulcanizing machine at a high pressure (15.0 MPa) at 185 ℃ for 3 min. After release pressure, the pressed sheet was taken out and cooled down in cold pressing machine at near zero pressure to keep flat.

Characterization

Morphologies of the P(VC-co-AAEM) and P(VC-co-AAEM)/ZnO particles were observed by using scanning electron microscopy (SEM, JSM-6700F, Hitachi, Japan). For the SEM observation, a few drops of the P(VC-co-AAEM) or P(VC-co-AAEM)/ZnO dispersion were diluted with deionized water and ultrasonicated for 30 min to obtain a translucent suspension. Then, a drop of the suspension was cast onto a conductive silicon wafer and dried under a reduced pressure overnight at room temperature. Another mode is a little dry P(VC-co-AAEM)/ZnO composite particles spread on silicon

wafer directly. After that, the samples were sputtered with a thin platinum layer prior to imaging.

The contents of oxygen and chlorine on the surface of P(VC-co-AAEM) particles were detected by X-ray photoelectron spectroscopy (XPS, Genesis 60S, EDAX, America).

The infrared spectrum of P(VC-co-AAEM) powder was recorded with Fourier transform infrared spectroscopy (FT-IR, Vector-22, Bruker, Germany). Prior to analysis, the dried sample was mixed with KBr, and pressed to form a tablet.

^{1}H nuclear magnetic resonance (NMR) characterization of P(VC-co-AAEM) and pure PVC was performed using an Avance400 NMR instrument (Bruker Biospin AG). Typically, a small amount of the copolymer sample after purified was dissolved in 0.5 mL of deuterated dimethyl sulfoxide.

GPC analysis of the P(VC-co-AAEM) template and pure PVC was performed on a Polymer Laboratories (PL) Series 220 high temperature chromatography, equipped with an column oven, and two PL gel columns (10 μm, mixed bed, 300×7.5 mm). THF (HPLC-grade; Kermel) was used as an eluent at a flow rate of 1 mL/min. The molecular weights (MW) and number-average molecular weight (M_n) were determined using PS standards. The sample preparation was as follows. The sample was first purified to remove probable impurity and insoluble substance. The as prepared P(VC-co-AAEM) copolymer was extracted by Soxhlet's apparatus using tetrahydrofuran as a solvent for 24 h. The dissolved P(VC-co-AAEM) was precipitated from the solution by reduced pressure distillation. Subsequently, the collected P(VC-co-AAEM) polymer was freeze-dried for 24 h. The obtained product was used for the GPC and NMR measurements.

The size distribution of P(VC-co-AAEM) particles in aqueous dispersion was analyzed with Zeta-Sizer 90 type of dynamic laser scattering particle size analyzer (DLS, Malvern, England). For preparing the sample characterized by DLS, a drop of the P(VC-co-AAEM) latex (0.03-0.04 g) was diluted with 12 mL of deionized water in a 15 mL glass tube and ultrasonicated for 30 min to obtain a translucent suspension, and the pH value of the dispersion was 6.8. The DLS measurement was performed at 25 ℃. The wavelength of incident light was 532 nm and the scattering angle was 90 °.

The ZnO powder and P(VC-co-AAEM)/ZnO composite were characterized by X-ray powder diffraction (XRD, D8 Focus, Bruker, Germany) in the 2θ range from 20 to 80 °, using a diffractometer equipped with a graphite monochromatized Cu Kα radiation (λ= 1.5405 Å). And energy-dispersive X-ray analysis (EDX) was carried out with X-ray analyser coupled with SEM (SEM, Nano 450, FEI, USA).

The contact angles of water droplet on the P(VC-co-AAEM) particle films were measured on a DSA30S instrument (KRÜSS Co., Germany) at room temperature. The films were obtained by this procedure that a few drops of P(VC-co-AAEM)/ZnO suspension were cast onto a glass slide for a thin layer and then dried in vacuum oven at room temperature for 12 h.

Thermal analysis of the composite samples for foaming was performed by differential scanning calorimetry (DSC, Diamond, Perkin Elmer, Germany) under a dry nitrogen atmosphere. Approximately 7.0 mg of sample was heated to 250 ℃ at a rate of 10 ℃ min^{-1}.

Thermogravimetric analysis (TGA) was performed by Perkin-Elmer TA Q-600 analyzer. P(VC-co-AAEM)/ZnO products were heated in platinum crucible at a heating rate of 10 ℃/min from room temperature up to 800 ℃ with air carrier gas of 100 mL min^{-1}.

SEM was used to characterize the pore sizes and their distribution in the foamed samples. The samples were frozen in liquid nitrogen and fractured to ensure that the microstructure remained clean and intact. Subsequent platinum coating provided the necessary conductive surface for the electron microscope study.

Results and discussion

Synthesis and Morphology of P(VC-co-AAEM) Nanoparticles

To prepare anisotropic P(VC-co-AAEM)/ZnO composite particles, monodisperse P(VC-co-AAEM) particles containing β-diketone groups on their surface were first prepared by surfactant-free emulsion polymerization. Here, the AAEM with hydrophilic character acts as both an emulsifier and a comonomer since it may stabilize the obtained colloidal system, and is preferentially located on the particle surface after the copolymerization with VC.[41,42] Fig. 1A shows the SEM image of the representative P(VC-co-AAEM) beads containing 10 wt% AAEM (from Sample b in Table1). It indicates that the size of P(VC-co-AAEM) particles is 280-290 nm following a very narrow diameter distribution (PDI=0.039), implying the possibility of the formation of isolated PAAEM particles is negligible in this system.

The incorporation of AAEM into PVC beads was confirmed by FT-IR spectroscopy. Fig. 1B demonstrates the FT-IR spectrum of the prepared P(VC-co-AAEM) particles. The absorption bands at 689 and 616 cm^{-1} can be assigned to the C-Cl stretching vibrations. [43] The strong peaks at 1430 and 1251 cm^{-1} can be attributed to the CH_2 bending vibration and the C-H bending vibration in CHCl, respectively.[44] Such absorption peaks are all attributed to the characteristic groups of PVC. At the same time, some other peaks also appear in the FT-IR spectrum. The strong absorption band displayed at 1728 cm^{-1} is typically assigned to the stretching vibration of carbonyl groups (-C=O) in the P(VC-co-AAEM) particles.[45] And the bands at 2969, 2912, and 2850 cm^{-1} are produced from the stretching vibration of saturated C-H groups.[46]The band at around 3435 cm^{-1} could be assigned to the -OH absorption of trace amount of water in KBr and during the sample preparation step. All above results indicate that the carbonyl groups derived from AAEM exist in the polymer latex particles. Thus, the tailored particles can serve as a template for preparing P(VC-co-AAEM)/ZnO nanocomposites successfully.

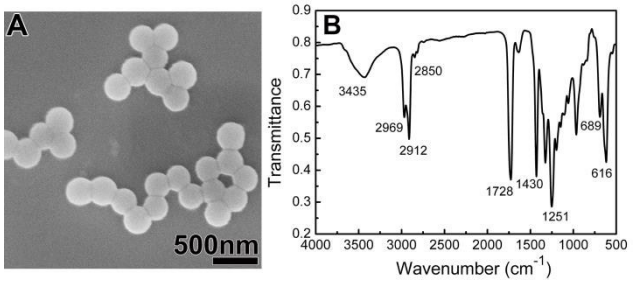

Fig. 1 SEM image (A) and FTIR spectrum (B) of the P(VC-co-AAEM) particles containing 10 wt% AAEM.

The successful synthesis of P(VC-co-AAEM) copolymer has also been confirmed by GPC and ^{1}H NMR techniques. The representative ^{1}H NMR spectra of the P(VC-co-AAEM) template and pure PVC for comparison are presented in Fig. 2A. From Fig. 2A, the ^{1}H NMR spectrum of pure PVC shows the broad signals at around 4.3-4.7 and 2.1-2.4 ppm corresponding to –CHCl and –CH_2 groups in the polyvinyl chloride chain segments, respectively.[47-49] However, in ^{1}H NMR spectrum of the P(VC-co-AAEM), new signals present at 1.2, 1.4-2.0, 3.75, 4.26, 5.30 and 5.36 ppm correspond to the absorption of –$C(CH_3)$, CH_2 in the copolymer main chain, –CO–CH_2–CO–, –CH_2–CH_2– and –CH=C(OH) groups in the AAEM unit segments, respectively.[50,51] The signals of methyl groups of ketones (–CO–CH_3) are overlapped in the region of 2.0-2.5 ppm. These characteristic signals indicate that the AAEM segments have been chemically bonded to polyvinyl chloride chains during the copolymerization process.

The GPC traces for the P(VC-co-AAEM) copolymer and pure PVC control were also measured, as shown in Fig. 2B. The molecular weight and its polydispersity (PD) of each polymer can be observed from Fig. 2B. The AAEM copolymerized VC resulted in the molecular weight of the copolymer shift towards lower value relative to the PVC homopolymer, and followed the decrease of PD value due to an incorporation of the AAEM comonomer. Additionally, it can be seen from Fig. 2B that the molecular weight distribution for the P(VC-co-AAEM) copolymer appeared unimodal, implying no evidence of homopolymer contamination during the copolymerization. These results by ^{1}H NMR, FT-IR, and GPC studies were strong evidences of successful preparation for the functionalized P(VC-co-AAEM) templating coplolymer.

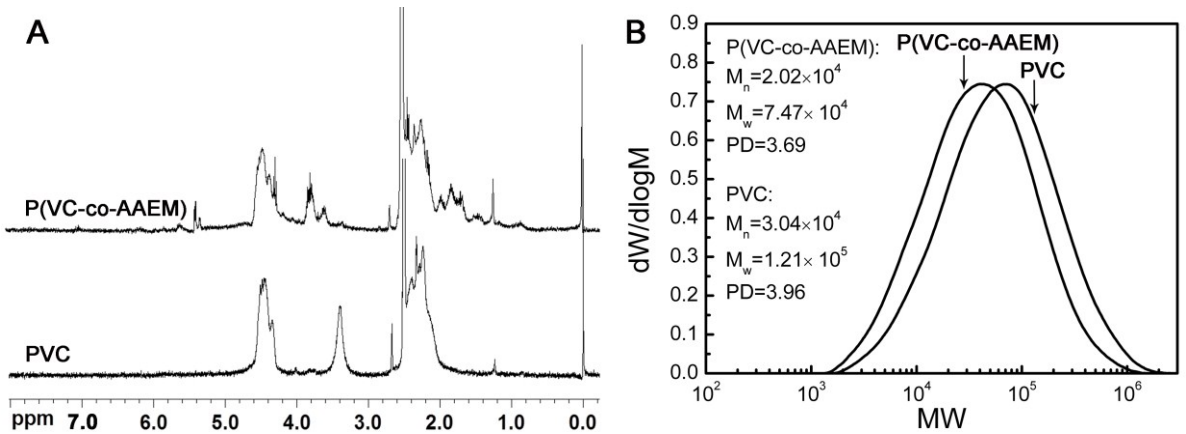

Fig. 2 ^{1}H NMR spectra and GPC traces of pure PVC and P(VC-co-AAEM)

Moreover, this system allows effective control of the content of β-diketone groups on the P(VC-co-AAEM) template surface by changing the amount of hydrophilic AAEM comonomer in the reaction mixture. To investigate the effect of AAEM feed ratio, we carried out four experiments with 0 to 20 wt% AAEM (based on VC monomer, as shown in Table 1). Detailed investigation of their hydrophilicity was performed by contact angle experiment. It can be observed from Fig. 3A that the contact angle of water droplet on the pure PVC particle film is 113.4 °. For the particle film with 10 wt% AAEM of P(VC-co-AAEM) copolymer, the contact angle drops distinctly to 78.4 °. It is obvious that the hydrophilicity of the particle film increases. When the films of P(VC-co-AAEM) particles prepared at the AAEM content of 15 wt% and 20 wt% are measured, the corresponding contact angles are 64.8 ° and 57.9 °, respectively (see Figs. 3C and D). Clearly, the hydrophilicity on the P(VC-co-AAEM) template surface can be enhanced by increasing the AAEM content, which has also been confirmed by XPS results below.

In our very recent work,[41] synthesis of anisotropic P(VC-co-AAEM)/PS nanoparticles also used the P(VC-co-AAEM) particles as template. We chose the XPS spectrum of the surface of the P(VC-co-AAEM) particles containing 10 wt% AAEM as a typical example. When the AAEM/VC ratio was 6.0 g/ 60.0 g, the content of oxygen in the P(VC-co-AAEM) particles surface was 6.65%, which was much higher than the calculated average content of oxygen (3.39%) in the P(VC-co-AAEM) particles. Adversely, the chlorine content (39.03%) in the template surface was much lower than the calculated average content of chlorine (51.64%) in the P(VC-co-AAEM). Those experimental results confirmed that the AAEM containing β-diketone was predominantly located onto the

particle surface during the copolymerization process of AAEM with VC. Clearly, the results by XPS study (see Fig. S1 in Supporting Information) are consistent with the contact angle measurement.

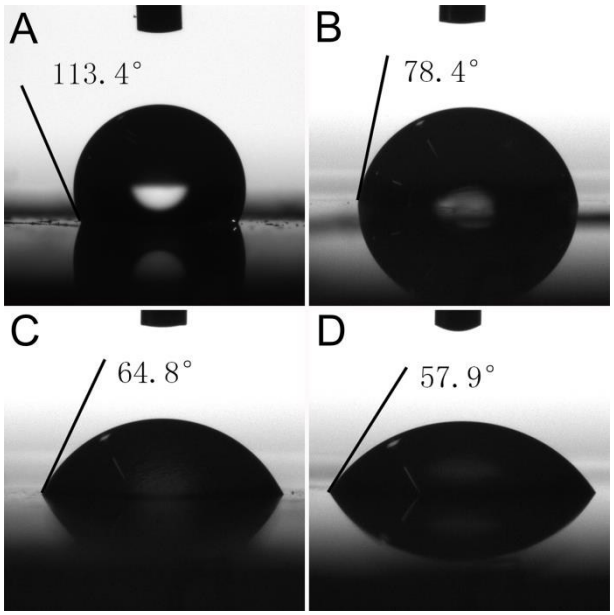

Fig. 3 Contact angles of water droplets on the P(VC-co-AAEM) polymer particle films. The corresponding AAEM content: (A) 0 wt%; (B) 10 wt%; (C) 15 wt%; (D) 20 wt%.

In addition, the average sizes and size distributions of P(VC-co-AAEM) particles tested by DLS are summarized in Table 1 and Fig. 4 to demonstrate the influence of different AAEM contents on the template preparation. From Table 1 and Fig. 4, all the size distribution of these P(VC-co-AAEM) particles present a single peak and near monodispersity, indicating there is not a self-polymerization of AAEM monomers during the copolymerization. Also, we can see the sizes of polymeric particles slightly decrease with increasing the amount of AAEM.[33]

Coating process of ZnO Particles

Fig. 5 shows X-ray diffraction patterns obtained from dry powder samples (set 1 in Table 2) with different reaction times. At 20 min of reaction, the spectrum (Fig. 5A) reveals the characteristic peak at 36.3° of ZnO crystal structure along with several other peaks. Before this test, sodium acetate was cleaned out by centrifugation and washing procedure, because it is only slightly soluble in IPA but more soluble in water (1.19 g mL^{-1}). As a result, there is no evidence of crystalline sodium acetate in the spectrum. The other peaks correspond to the precursor for the synthesis of ZnO. The nature of the precursor is expected to be strongly dependent on the relative conditions.[52] It has been reported in the literature that the formation of positively charged complexes such as $[ZnL_h(OH_2)_{N-h}]^{(2-h)+}$ precedes nucleation and growth processes of ZnO nanocrystals.[53,54] This structure, often called hydroxy double salt (HDS) structure, is characterized by sheets of composition $[Zn_3{}^{oct}(OH)_8Zn_2{}^{tetr}(H_2O)_2]^{2+}$ in which zinc atoms occur in both octahedral and tetrahedral coordination. These phenomena imply that the precursors have not converted into ZnO nanocrystals completely. After 1 h, we note that the characteristic peaks of ZnO nanocrystals are distinctly sharp and clear. Fig. 5B shows main peaks at 2θ= 31.9°, 34.4°, 36.3°, 47.5°, 56.7°, 62.9°, corresponding to (100), (002), (101), (102), (110), (103) planes, respectively. All diffraction peaks for the synthesized ZnO nanocrystals exhibit the characteristic peaks of crystalline ZnO with wurtzite structure, which are consistent with the standard values for bulk ZnO (JCPDS card 36-1451).[52] From the results above, it can be concluded that pure ZnO has been successfully synthesized after 1 h.

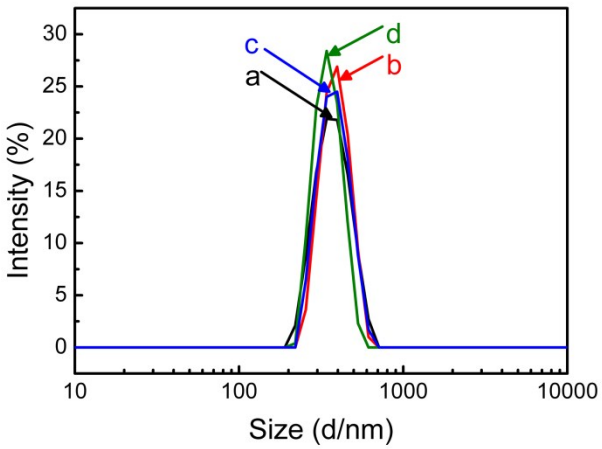

Fig. 4 Size distributions of P(VC-co-AAEM) particles in Table 1: the content of AAEM was (a) 0 wt%, (b)10 wt%, (c)15 wt%, (d) 20 wt%.

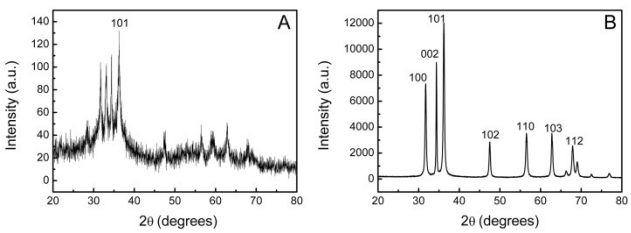

Fig. 5 X-ray diffraction patterns for the growth of ZnO nanocrystals by reacting for: (A) 20 min, (B) 1 h. Synthesis condition: 2 mL of 0.2 M aqueous NaOH solution, 2.0 mM $Zn(Ac)_2{\bullet}2H_2O$, and 80 mL of IPA at 55 ℃.

P(VC-co-AAEM)/ZnO composite particles were synthesized by *in situ* coating ZnO nanocrystal on the surface of functionalized P(VC-co-AAEM) beads. The driving force for the formation of the P(VC-co-AAEM)/ZnO composite particles is considered to be the electrostatic interactions between the electron-rich β-diketone groups located on the surface of P(VC-co-AAEM) cores and the electron-deficient ZnO precursors in IPA solution. As we know, Agrawal reported the preparation of polystyrene-ZnO composite particles by templating the ZnO nanocrystals against the functionalized polymeric core.[33] In this

work, the PVC beads with 10 wt% content of AAEM are mainly used as the template for the deposition of ZnO nanocrystals. Thus, the P(VC-co-AAEM) core should have an important effect on morphology and content of ZnO nanocrystals for the hybrid composite particles. And then our interest is to study the effect of the template particles on formation of ZnO nanocrystals.

For better understanding the combination between ZnO nanocrystals and P(VC-co-AAEM) beads, the mechanism of formation for ZnO is described in detail herein. According to the literature,[33] the formation of ZnO nanocrystals consists of three different stages: (a) the formation of precursor for ZnO nanocrystals in the medium, (b) nucleation and growth processes of ZnO nanocrystals after adding hydroxyl ions, and (c) coarsening and aggregation of nanoparticles. The difference from pure ZnO nanocrystals' synthesis is that functionalized surfactant-free P(VC-co-AAEM) particles was added in mixture after $Zn(Ac)_2$ solution refluxing for 1h, ZnO precursors interacted immediately with β-diketone groups which presented on the surface of PVC beads. Just after injection of NaOH aqueous solution, sample aliquots were taken from the reacting mixture at preset time intervals throughout the formation process of P(VC-co-AAEM)/ZnO composite particles. The products were studied by XRD for crystalline structures of the composite particles.

It can be seen from Fig. 6A that the Zn-HDS exists at 1 h of reaction, and as shown in Fig. 6B, the Zn-HDS is also observed upon reaction for 3 h. However, as the reaction goes on, the characteristic X-ray diffraction of ZnO become increasingly sharp. As displayed in Fig. 6C, when the reaction time prolongs to 4 h, the diffraction pattern exhibits the characteristic zincite peaks while no evidence of precursors. At 6 h, the intensity and peak shape of the diffraction pattern almost don't change. Compared with the JCPDS card 36-1451, the spectrum in Fig. 6C confirms the purity and crystalline nature of ZnO coated on the polymeric core, suggesting that crystal structure of ZnO is not altered by the presence of functionalized polyvinyl chloride. From Figs. 5 and 6, we can see that the intense peaks of ZnO precursor disappear, indicating nucleation and growth of ZnO crystal in the presence of the P(VC-co-AAEM) particles are completed after about 4 h. In contrast, the nucleation and growth of ZnO in the absence of the template are completed in less than 1 h. Obviously, the addition of functionalized particles in the reaction system delays the formation of ZnO nanocrystals. This can be explained as follows:

In this system, the formation of ZnO nanocrystals could occur in two sites due to an addition of the PVC template beads. One part of ZnO precursors nucleate in the reaction media, namely homogeneous nucleation. Another part of ZnO precursors nucleate on the polymer beads in consequence of the interaction between active sites (β-diketone groups) and ZnO precursors, namely heterogeneous nucleation. As a result of both competition, the heterogeneous nucleation of hybrid composite particles dominates due to its lower energy barrier, which is expected according to Scheme 1b. The addition of sodium hydroxide provokes the nucleation of ZnO precursors on the polymer surface. Clearly, the movement of ZnO precursors anchoring PVC beads could slow down due to its large size in comparison with the free ZnO precursor in the solvent, and the chance of hydroxide ion transfer to polymer surface decreases, leading to the delay of formation of ZnO nanocrystals.

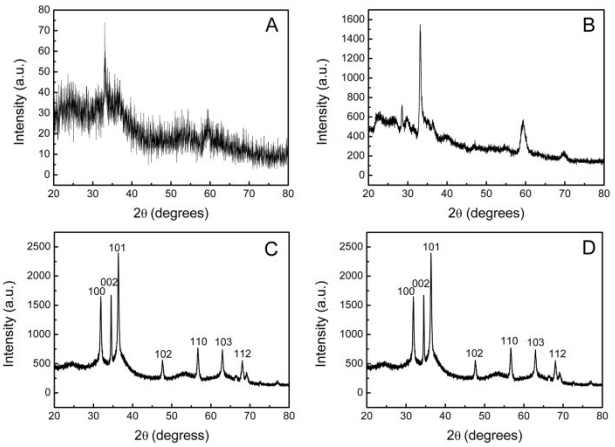

Fig. 6 XRD spectra of P(VC-co-AAEM)/ZnO nanocomposite prepared at the reaction time of (A) 1 h, (B) 3 h, (C) 4 h and (D) 6 h by using 2 mL of 0.2 M aqueous NaOH solution, 2.0mM $Zn(Ac)_2$•$2H_2O$, 0.45 g of the template particles containing 10% AAEM, and 80 mL of IPA at 55 ℃.

FT-IR spectroscopy can be used to confirm the characteristic functional groups of P(VC-co-AAEM)/ZnO composite nanoparticles, and further the interaction of ZnO with β-diketone groups, located on the surface of P(VC-co-AAEM) beads. Fig. 7 shows FT-IR spectra of the P(VC-co-AAEM)/ZnO particles and the corresponding P(VC-co-AAEM) template. The characteristic peak at 1728 cm^{-1} can be assigned to the strong stretching vibration of carbonyl groups (C=O) in the P(VC-co-AAEM) copolymer. The appearance of the C=O stretching band at 1575 cm^{-1} and the C-O stretching band at 1387 cm^{-1} is undoubtedly attributed to the acetate groups present on the ZnO particle surface.[33,55] The C-O stretching band at 1425 cm^{-1} for the acetate groups on ZnO surface overlaps with the peak at 1430 cm^{-1} produced from the bending vibration of methylene group. The evidence indicates that the above-mentioned procedure cannot remove acetate groups from ZnO surface, and the unidentate type of bonding structure (or coordination mode) for acetate group with metal (zinc) is observed in the FT-IR spectrum of the as-prepared P(VC-co-AAEM)/ZnO.[55] Also, it can be observed from Fig. 7 that the intensity of the peak at 1728 cm^{-1} decreases significantly due to an incorporation of the deposited ZnO nanoparticles.[45]

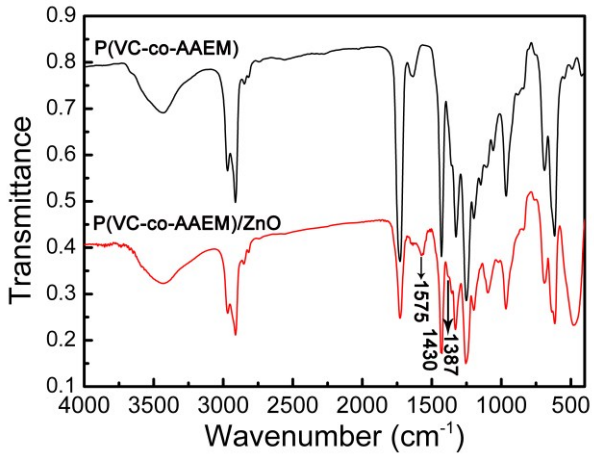

Fig. 7 FT-IR spectra of as-prepared P(VC-co-AAEM)/ZnO composite particles and the corresponding P(VC-co-AAEM) template.

Effect of AAEM Content

To clearly investigate the effect of β-diketone groups on the morphology of formed P(VC-co-AAEM)/ZnO composite particles, the effect of AAEM content is first studied. Here, we carried out synthesis of the composite particles using the P(VC-co-AAEM) beads with different AAEM contents (0 to 20 wt%) as the templates (shown in Table 1). And the reaction temperature of 55 ℃ and reaction time of 4 h were applied in all following syntheses. Fig. 8 shows the SEM images of the composite particles by using CBS probe in field emission SEM. Two procedures of sample preparation for the SEM observation are taken. The images on the left are obtained from the powder samples, and the images on the right come from the suspensions. From Figs. 8A to F, one can observe the deposition of islands of ZnO nanocrystals on the surface of templates leading to a raspberry-like morphology, and the agglomerates of ZnO crystal are spherical with a diameter of 5-40 nm. Increasing AAEM content in the P(VC-AAEM) particles causes increasing amount of ZnO nanoparticles to deposit on the template surfaces. Upon increasing the AAEM content to 20 wt% results in formation of the morphology with uneven and defective ZnO sheet covering the template surface (Fig. 8 G and H). This change in morphology with increasing AAEM content can be explained as follows: As we know, the interaction is established between ZnO precursors and functionalized polymer surfaces before nucleation in the reaction media. Once nucleation is formed on the surfaces of polymer beads, the growth of formed nuclei is followed. Herein, we consider that there are two possible modes of describing the growth of ZnO crystals, *i.e.* (i) classical Ostwald growth and aggregation; (ii) oriented attachment mechanism.[56] In Ostwald growth process, the formation of tiny crystalline nuclei in a supersaturated medium occurs first, and subsequent is crystal growth, in which the larger particles will grow at the cost of the smaller ones due to both higher solubility energy difference based on the Gibbs-Thompson law. It could be that, as soon as the smallest stable molecular clusters (they may be unit cells) are formed, they will rapidly grow to give the next most stable primary aggregate by combining with smaller unstable nuclei rather than by colliding with other stable particles. These primary aggregates would further rapidly combine to give the next most stable secondary aggregate and so on. And thus spherical ZnO nanocrystals are formed on PVC beads due to a fraction of the active sites (β-diketone groups) available on the template surface. With increasing AAEM content from 0 to 15 wt% in the P(VC-co-AAEM), the available active sites interacted with ZnO precursors increase, resulting in more ZnO nanocrystals nucleating on the PVC beads to form raspberry-like morphology. In contrast, pure PVC beads (without AAEM) are coated only with a spot of ZnO particles rather than none (see Fig. 8A and B). This is because PVC is polar polymer, which only has very weak interaction with electron-deficient ZnO precursors.

Whereas the content of AAEM reaches certain critical value, such as 20 wt% of AAEM content, all the surfaces of PVC beads are almost covered by the available active sites, which have interacted with ZnO precursors, and hence the nucleation sites of ZnO nanocrystals increase greatly. This prevents much tiny ZnO crystals further aggregation. As a result, the PVC beads are coated with a great deal of smaller ZnO crystal to form near complete wrapping of composite particles rather than raspberry-like shape. At the given amount of $Zn(Ac)_2 \cdot 2H_2O$, the concentration of Zn ion is not enough to coat all the surface of functionalized PVC beads. Ultimately, a defective ZnO coating is constructed on the PVC beads (Fig. 8G and H). Clearly, Ostwald ripening mechanism cannot explain this phenomenon well. We consider that ZnO crystal growth mode is changed due to intensive nucleation sites. The larger ZnO crystals grow from small primary nanoparticles through new mechanism of an oriented attachment in this system. The adjacent nanoparticles are self-assembled by sharing a common crystallographic orientation and docking of these particles at a planar interface. From the thermodynamic viewpoint, the driving force for this spontaneous oriented attachment is that the elimination of the pairs of high energy surfaces will lead to a substantial reduction in the surface free energy.[57] Nevertheless, this system cannot completely exclude the possibility of Ostwald ripening mechanism based on the SEM observation result. Consequently, the shape of ZnO changes from spherical particle to thin coating layer with increasing AAEM content in the template.

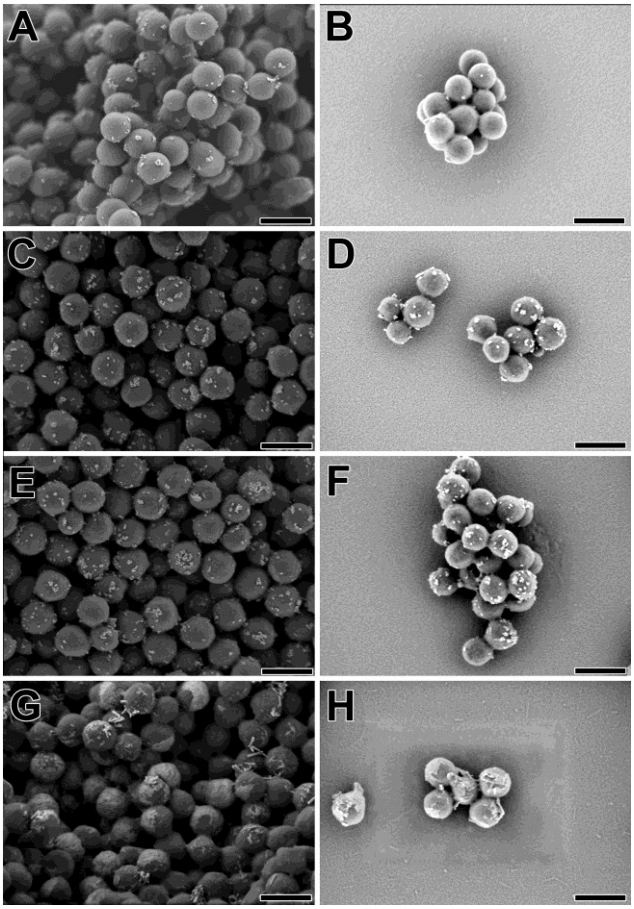

Fig. 8 SEM images of P(VC-co-AAEM)/ZnO particles prepared by using (A, B) 0 wt%; (C, D) 10 wt%; (E, F) 15 wt%; (G, H) 20 wt% AAEM content of P(VC-co-AAEM) beads, respectively. The images on the left obtained from the powder samples, and the images on the right from the suspensions. Scale bar: 500nm.

EDX analysis has been used for determination of the chemical compositions of particle surface. Fig. 9 shows a result of a complex EDX analysis performed for the sample P(VC-co-AAEM)/ZnO raspberry-like particles (obtained from set 4 in Table 2). Fig. 9A demonstrates the SEM image of the sample indicating the spots selected for EDX analysis. The P(VC-co-AAEM)/ZnO particles are randomly distributed on the Si support in one plane. Two small bulges on the surface of the raspberry-like composite particles have been selected as sites for the spot scan. For easy discernment, a clear same SEM image is also shown in Fig. 9B. Fig. 9 C and D display the EDX spectra of the sample spots investigated during the spot-scan, indicating the strongest signals related to Si (derived from support), Zn, and O. These data further confirm the clear presence of ZnO nanocrystals as small nanoparticles or islands on the template surface.

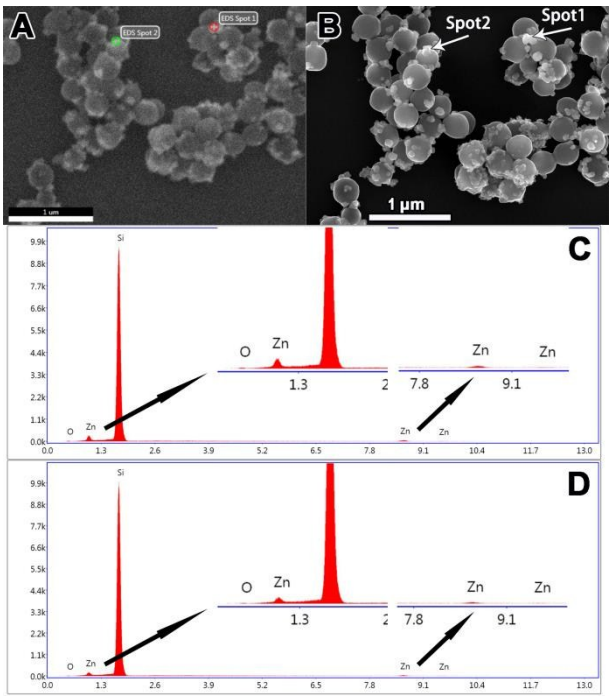

Fig. 9 The SEM image of P(VC-co-AAEM)/ZnO composite nanoparticles (prepared from set 4 in Table 2) indicating the spots selected for EDX analysis (spots show the sites on the raspberry-like particles by the spot scan) (A); the same clear SEM image (B); corresponding EDX spectra of spot 1(C) and spot 2(D).

Effect of NaOH concentration

According to the literature[52], the concentration of NaOH aqueous solution was found to influence the nucleation and growth processes of ZnO nanocrystals to a great extent. Consequently, it would induce distinct impact on the size and morphology of *in situ* formed composite particles. The P(VC-co-AAEM) particles with 10 wt% AAEM content were used to prepare hybrid composite particles in this case.

Fig. 10 shows the SEM images of the composite particles prepared at different NaOH concentrations. From these images, one can observe the typical raspberry-like morphology of composite particles in all cases and an increasing size of agglomerates of ZnO nanocrystals deposit on the surface of PVC beads with increasing NaOH concentration (from 0.2 to 1.0 M). At lower NaOH concentration (0.2 M), relatively small agglomerates of ZnO nanocrystals distribute discretely on the surface of PVC beads. Whereas increasing the NaOH concentration to 1.0 M, relatively large agglomerates of ZnO nanocrystals are formed on the template surface. Because an increment of NaOH concentration accelerates the hydrolysis of $Zn(Ac)_2{\cdot}2H_2O$, the rates of nucleation and growth of ZnO nanocrystals are enhanced significantly. Consequently more amount of ZnO precursors begin to nucleate on the template surface at the given reaction time. Also, it has been reported that increasing the NaOH concentration leads to a coarsening effect of ZnO nanocrystals because the solubility of zinc species is increased in the reaction media. This coarsening

process involves the growth of larger particles at the expense of smaller particles, and is further enhanced with increasing hydroxyl ion concentration in reaction media.[33] Thus, at higher NaOH concentration (1.0 M), it can be seen that the deposition of islands of relatively larger ZnO nanocrystals on the surface of templates results in the raspberry-like morphology due to the coarsening process. Whereas at lower NaOH concentrations (0.2 M), the slow nucleation and growth processes of ZnO nanocrystals as well as the suppressed effect of coarsening allow the coating of relatively smaller ZnO nanocrystals on the surface of templates within 4 h. Therefore, we can facilely tune the size and number of ZnO nanocrystals on PVC beads within raspberry-like morphology by adjusting the concentration of NaOH solution.

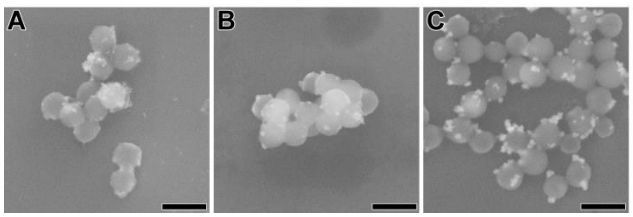

Fig.10 SEM images of P(VC-co-AAEM)/ZnO composite particles prepared at A) 0.2, B) 0.5, C) 1.0 M NaOH solution (2 ml) by using 2.0 mM $Zn(Ac)_2$•$2H_2O$ and 80 mL of IPA. Scale bar: 500nm.

Effect of $Zn(Ac)_2$•$2H_2O$ Amount

To investigate the effect of reactant feed amount, the morphologies of P(VC-co-AAEM)/ZnO composite particles prepared at different feed amount (sets 2-5 in Table 2) were also studied by SEM observation. Fig. 11 reveals that the number of agglomerates of ZnO nanocrystals deposited on the P(VC-co-AAEM) beads is increased with increasing substance amount of NaOH and $Zn(Ac)_2$•$2H_2O$, whereas the size of agglomerates of ZnO nanocrystals decreases. This could be attributed to two main factors: one is the increasing molar number of $Zn(Ac)_2$•$2H_2O$ in the reaction mixture, and the other one is the prolonged feed time of aqueous NaOH solution for the given concentration and dropping rate.

Fig. 11A illustrates the raspberry-like morphology of composite particles with a few large ZnO nanocrystals in about 50-100 nm of sizes deposit on the PVC beads. This can be explained as follows. At lower addition amount of NaOH and $Zn(Ac)_2$•$2H_2O$, the formation of few ZnO nanocrystals on the template dominates, and then leads to a coarsening process, which involves the growth of larger particles after adsorbing smaller unstable particles. Thereby larger size of ZnO nanocrystals is produced discretely on the given PVC beads. Following the similar reason, Fig. 11B demonstrates the P(VC-co-AAEM)/ZnO hybrid particles with moderate size and amount of ZnO nanocrystals available on the bead surface.

Different a bit from the above results, Fig. 11C and D reveals that the raspberry-like morphology of composite particles with smaller size and much number of ZnO nanocrystals are densely anchored on the template surface at higher addition amount of NaOH and $Zn(Ac)_2$•$2H_2O$. This is because the lower concentration of template particles (*i.e.* the fixed 0.45 g of latex particles dispersed in up to 400 mL of IPA from set 5 in Table 2) and the extension addition time of the NaOH solution (40 min) at a fixed concentration and feed rate largely delay the nucleation of ZnO. As a result, the coarsening process doesn't occur in the specific reaction time (4 h). In addition, because more ZnO precursors produce in the reaction medium and interact with the functionalized polymer beads, the nucleation can occur at the more active sites. And then the raspberry-like nanocomposite particles with smaller and richer ZnO nanocrystals deposited on the PVC beads are achieved due to the combined effect of the above two factors.

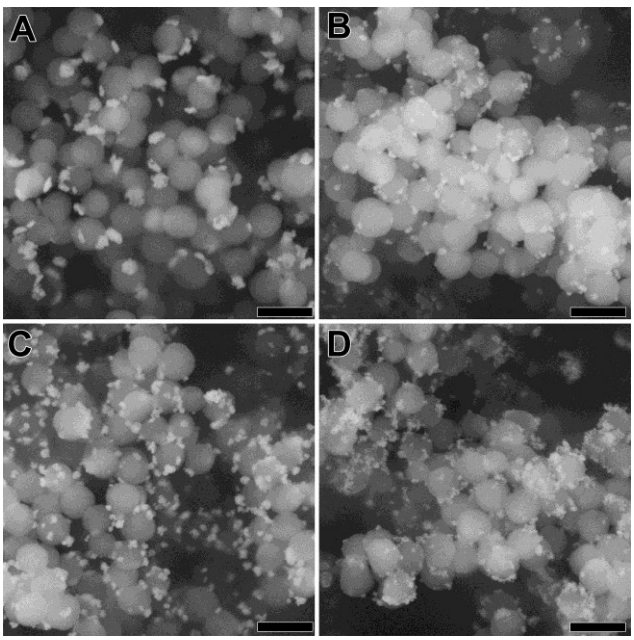

Fig. 11 SEM images of P(VC-co-AAEM)/ZnO nanocomposite prepared by using set 2, 3, 4 and 5 in Table 2, corresponding to A, B, C and D. Scale bar: 500nm.

P(VC-co-AAEM)/ZnO Nanocomposite Modified with ADC for Foaming

In this foaming process, the synthesized PVC containing 10 wt% AAEM (sample no. b in Table 1) was used as a foaming matrix. ADC is well known to promote foam formation by decomposing at 210-220 ℃ and releasing a large volume of nitrogen, carbon monoxide and carbon dioxide.[58] To study the decomposition temperature of ADC in the composite particles obtained by Scheme 1c procedure, thermal behavior of the P(VC-co-AAEM)/ZnO composite particles modified via adsorbing ADC blowing agent (sample A) was characterized by using DSC (Fig. 12). At the same time, the corresponding TGA results are shown in Fig. S3 in the Supporting Information. For comparison, the blend (sample B) via mixing PVC powder, ZnO with ADC was characterized as well. The real mass ratio of PVC/ADC/ZnO in sample A was determined by TGA and

element analysis (see Fig. S2 and Table S1 in the Supporting Information). The content of ZnO measured by TGA in air atmosphere was ca. 2 wt%. The element analysis of sample A shows that the C, H and N contents therein were 37.00, 4.72 and 2.83 wt%, respectively. After calculation, the mass ratio of PVC/ADC/ZnO was found at near 100 g: 6 g: 2g (this detailed calculation procedure being also demonstrated in Supporting Information). And hence the control (sample B) was prepared with the same mass ratio.

It can be seen from Fig. 12 that the decomposition temperature of sample A locates between 176 ℃ and 203 ℃, while that of sample B locates between 184 ℃ and 210 ℃. Evidently, the ZnO has an important effect on the ADC decomposition temperature, which decreases the onset decomposition temperature of ADC beyond 30 ℃, depending on the compositions, mode and conditions of fabricating samples.[59-60] Thus, the as-prepared product can be desirable to manufacture PVC foam since the decomposition temperature of the blowing agent in the nanocomposite is close to the plasticizing temperature of PVC matrix.

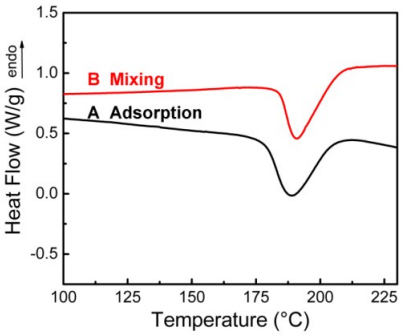

Fig. 12 DSC curves of A) dissolving ADC into P(VC-co-AAEM)/ZnO composite; B) blend of PVC, ZnO and ADC.

Furthermore, sample A shows a little lower decomposition temperature than sample B at the same ZnO content, which is attributed to different preparation method. The ADC blowing agent in sample A, after dissolved and adsorbed treatment, shows better dispersion in the PVC/ZnO nanocomposite than in sample B prepared via a traditional simple mixing of the used raw materials, making ZnO nanoparticles contact ADC more closer. Namely, ZnO nanocrystal has better effect on decreasing the decomposition temperature of ADC blowing agent. As a result, the modified composite nanoparticles are promising for foaming of PVC.

PVC foams corresponding to samples A and B were fabricated at 15 MPa and 185 ℃ for 3 min. The internal pore configuration of the PVC foams was obtained by SEM observation. From Fig. 13 and as shown in Fig. S4, Fig. S5, and Table S2 in Supporting Information, it can be observed that the pores in sample A appear the sizes at nanometer scale, and its average cell size was 101 nm. In contrast, the sample B shows not only a micrometer scale of cell sizes, which has an average pore size of 50.2 μm, but also even exhibits a few brittle caves (Fig. 13B). The difference largely derives from the unique advantage of our present method to prepare foam material. The ZnO nanoparticles deposited at the surface of the PVC beads should show better dispersion in the PVC matrix in comparison with the conventional blending mode, and the ADC blowing agent can be relatively homogeneously attached onto PVC/ZnO composite particles due to above adsorbing action. As a result, the ADC contacts closely and uniformly with ZnO nanoparticles. The well-dispersed ZnO nanoparticles into the polymer matrix may serve as nucleation sites to facilitate the bubble nucleation process. It is evidence that the cell density in the sample A foam (3.8×10^{13} cells/ cm^3) is much larger than that in the sample B foam (5.4×10^{6} cells/ cm^3) (shown in Table S2). Thus the pores in sample A are smaller and more intensive than those in sample B. However, to achieve a demand nanoporous structure, specific reaction parameters and processing factors, such as foaming temperature, foaming pressure *etc*., need further optimization. And the tendency of pore collapse will be controlled in future experiments.

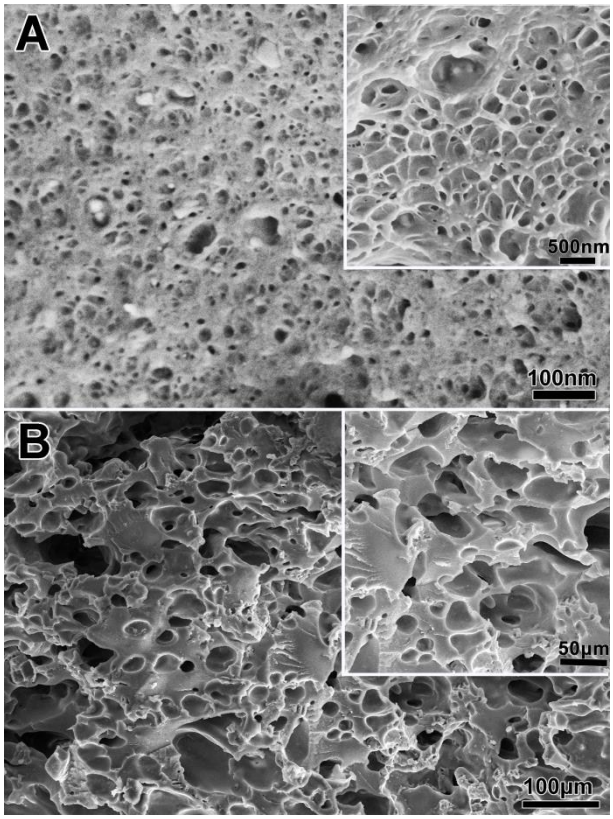

Fig. 13 SEM micrographs of the fractured surfaces of A) foaming sample using the PVC/ZnO composite adsorbed with ADC, B) foaming sample with the blend of PVC, ADC and ZnO, as the mass ratio of PVC: ADC: ZnO being 100 g: 6 g: 2 g. The insets in Fig. 13 were the SEM photos with each higher magnification.

Conclusions

Hybrid P(VC-co-AAEM)/ZnO nanocomposite particles with raspberry-like morphology have been fabricated through a

facile approach of surface heterogeneous nucleation. It has been proposed that the interaction between ZnO precursors and β-diketone groups contained in AAEM as a driving force is utilized for the formation of the hybrid particles. And the content of β-diketone groups can tune the size and morphology of nano-ZnO particles deposited on the template surface. Whereas at 20 wt% AAEM content, the morphology of P(VC-co-AAEM)/ZnO nanocomposite particles transformed raspberry-like shape into incomplete wrapping structure of the core, and the corresponding growth mechanism of ZnO crystals transformed classical Ostwald ripening mechanism towards a new oriented attachment mechanism. The incorporation of functionalized PVC beads slowed down the nucleation and growth rates of ZnO crystals, but didn't alter the crystal structure of ZnO. Moreover, NaOH concentration and feed amount of reactant played important roles in the development of ZnO on the PVC beads. The increment of either NaOH concentration or feed amount of reactants was found to bring about larger or more aggregates of ZnO nanocrystals deposition on the template. In particular, increasing the NaOH concentration caused the solubility of zinc species in the reaction media to increase, which successively enhanced the coarsening-effect of ZnO particles and accordingly leaded to the deposition of large aggregates on the template surface.

To our knowledge, raspberry-like particles can find extensive applications, for example, as a carrier of ZnO nanoparticles incorporated into suitable polymer matrices to obtain ZnO nanoparticles with better dispersion compared to the conventional blend. In addition, the composite particles produced are envisioned to have applications as the building blocks for fabrication of sensors, transducers, actuators, UV detectors, and optoelectronic devices.[33] Herein, beyond their interesting morphologies and combined the unique physicochemical properties of polymer with inorganic components, as-prepared P(VC-co-AAEM)/ZnO composites probably have potential application in nanofoam materials. The polymer foam with nanoporous structure has good mechanical strength including grip nail strength, high compressive strength, and thermal insulation properties in building engineering, while comparing with the polymeric foam having large pore sizes at micrometer scale and inhomogeneous pore size distribution.[61-63] The improved thermal insulation performance could be attributed to the nanometer pore structure allowing for lower thermal conductivity.[64] This research on specific application of the hybrid particles is currently underway. Furthermore, the versatile process can be used as a methodology to prepare other organic–inorganic hybrids, and by changing polymeric templates and precursors of inorganic nanoparticles can achieve certain desired characteristics.

Acknowledgements

Financial support for this work was received from the National Natural Science Foundation of China (Project no. 51373047) and the Hebei Province Natural Science Fund (B2012202131).

Notes and references

[a] *Institute of Polymer Science and Engineering, Hebei University of Technology, Tianjin 300130, P. R. China. Tel: +86-22-60202054. E-mail: mwpan@126.com*

[b] *College of Polymer Science and Engineering, State Key Laboratory of Polymer Materials Engineering, Sichuan University, Chengdu 610065, Sichuan, P. R. China. E-mail: ganji.zhong@scu.edu.cn*

[1] C. Sanchez, P. Belleville, M. Popall and L. Nicole, *Chem. Soc. Rev.*, 2011, **40**, 696.

[2] P. Judeinstein and C. Sanchez, *J. Mater. Chem.*, 1996, **6**, 511.

[3] C. Sanchez, B. Julián, P. Belleville and M. Popall, *J. Mater. Chem.*, 2005, **15**, 3559.

[4] M. Chen, S. X. Zhou, B. You and L. M. Wu, *Macromolecules*, 2005, **38**, 6411.

[5] J. Zhou, M. Chen, X. G. Qiao and L. M. Wu, *Langmuir*, 2006, **22**, 10175.

[6] Y. F. Wu, Y. Zhang, J. X. Xu, M. Chen, L. M. Wu, *J. Colloid Interface Sci.*, 2010, **343**, 18.

[7] R. K. Wang, H. R. Liu, F. W. Wang, *Langmuir*, 2013, **29**, 11440.

[8] F. W. Wang, H. R. Liu, Y. Zhang, H. W. Liu, X. W. Ge, X. Y. Zhang, *J. Polym. Sci., Part A: Polym. Chem.*, 2014, **52**, 339.

[9] Y. Chen, H. L. Yang, C. L. Zhang, Q. Wang, X. Z. Qu, J. L. Li, F. X. Liang and Z. Z. Yang, *Macromolecules*, 2013, **46**, 4126.

[10] T. Ge, L. Kuai, B. Y. Geng, *J. Alloys Compd.*, 2011, **509**, 353.

[11] T. T. Zhuang, F. J. Fan, M. Gong and S. H. Yu, *Chem. Commun.*, 2012, **48**, 9762.

[12] D. Mouleeswaran, R. Dhanasekaran, *Mater. Sci. Eng., B*, 2006, **130**, 137.

[13] M. B. Dickerson, S. E. Jones, Y. Cai, G. Ahmad, R. R. Naik, N. Kröger, and K. H. Sandhage, *Chem. Mater.*, 2008, **20**, 1578.

[14] B. Weintraub, Z. Z. Zhou, Y. H. Li and Y. L. Deng, *Nanoscale*, 2010, **2**, 1573.

[15] V. M. Bogatyrev, V. M. Gun'ko, M. V. Galaburda, M. V. Borysenko, V. A. Pokrovskiy, O. I. Oranska, E. V. Polshin, O. M. Korduban, R. Leboda, J. Skubiszewska-Zięba, *J. Colloid Interface Sci.*, 2009, **338**, 376.

[16] A. A. Montaser, P. Veluchamy, H. Minoura, *J. Electroanal. Chem.*, 1996, **419**, 47.

[17] A. Pich, S. Bhattacharya, H. -J. P. Adler, *Polymer*, 2005, **46**, 1077.

[18] R. Khan, A. Kaushik, P. R. Solanki, A. A. Ansari, M. K. Pandey, B. D. Malhotra, *Anal. Chim. Acta*, 2008, **616**, 207.

[19] S. H. Wei, S. M. Wang, Y. Zhang, M. H. Zhou, *Sens. Actuators, B*, 2014, **192**, 480.

[20] I. S. Yahia, A. A. M. Farag, M. Cavas, F. Yakuphanoglu, *Superlattices Microstruct.*, 2013, **53**, 63.

[21] D. Wu, W. Wang, F. T. Tan, F. Z. Sun, H. F. Lu and X. L. Qiao, *RSC Adv.*, 2013, **3**, 20054.

[22] F. Tamaddon, S. Moradi, *J. Mol. Catal. A: Chem.*, 2013, **370**, 117.

[23] T. O. Okyay, R. K. Bala, H. N. Nguyen, R. Atalay, Y. Bayam and D. F. Rodrigues, *RSC Adv.*, 2015, **5**, 2568.

[24] Y. Ge, J. P. Schimel, and P. A. Holden, *Environ. Sci. Technol.*, 2011, **45**, 1659.

[25] E. J. Tang, G. X. Cheng, X. S. Pang, X. L. Ma, F. B. Xing, *Colloid. Polym. Sci.*, 2006, **284**, 422.

[26] Y. Tu, L. Zhou, Y. Z. Jin, C. Gao, Z. Z. Ye, Y. F. Yang and Q. L. Wang, *J. Mater. Chem.*, 2010, **20**, 1594.
[27] Z. P. Mao, X. L. Yu, L. P. Zhang, Y. Zhong, H. Xu, *Vacuum*, 2014, **104**, 111.
[28] A. L. Briseno, T. W. Holcombe, A. I. Boukai, E. C. Garnett, S. W. Shelton, J. J. M. Fréchet, and P. D. Yang, *Nano Lett.*, 2010, **10**, 334.
[29] L. Wang, X. H. Zhang and K. Z. Chen, *CrystEngComm*, 2013, **15**, 4860.
[30] E. J. Tang, S. Y. Dong, *Colloid. Polym. Sci.*, 2009, **287**, 1025.
[31] S. C. Liufu, H. N. Xiao, Y. P. Li, *Polym. Degrad. Stab.*, 2005, **87**, 103.
[32] Y. J. He, *Powder Technol.*, 2004, **147**, 59.
[33] M. Agrawal, A. Pich, N. E. Zafeiropoulos, S. Gupta, J. Pionteck, F. Simon, and M. Stamm, *Chem. Mater.*, 2007, **19**, 1845.
[34] M. Agrawal, N. E. Zafeiropoulos, S. Gupta, E. Svetushkina, J. Pionteck, A. Pich, M. Stamm, *Macromol. Rapid Commun.*, 2010, **31**, 405.
[35] M. W. Pan, L. Y. Yang, J. C. Wang, S. D. Tang, G. J. Zhong, R. Su, M. K. Sen, M. K. Endoh, T. Koga, and L. Zhu, *Macromolecules*, 2014, **47**, 2632.
[36] M. W. Pan, L. Y. Yang, B. Guan, M. S. Lu, G. J. Zhong and L. Zhu, *Soft Matter*, 2011, **7**, 11187.
[37] E. Şahin, F. Y. Mahlicli, S. Yetgin, D. Balköse, *J. Appl. Polym. Sci.*, 2012, **125**, 1448.
[38] N. Petchwattana, S. Covavisaruch, *Mater. Des.*, 2011, **32**, 2844.
[39] T. Sugimoto, *Adv. Colloid Interface Sci.*, 1987, **28**, 65.
[40] Z. S. Hu, G. Oskam, R. L. Penn, N. Pesika, and P. C. Searson, *J. Phys. Chem. B*, 2003, **107**, 3124.
[41] Q. Niu, M. W. Pan, J. F. Yuan, X. Liu, X. M. Wang and H. F. Yu, *Macromol. Rapid Commun.*, 2013, **34**, 1363.
[42] X. Liu, M. W. Pan, J. F. Yuan, Q. Niu, X. M. Wang and K. C. Zhang, *RSC Adv.*, 2014, **4**, 4163.
[43] X. Xiao, Z. G. Zeng, S. W. Xiao, *J. Hazard. Mater.*, 2008, **15**, 118.
[44] H. R. Jung, W. J. Lee, *Electrochim. Acta*, 2011, **58**, 674.
[45] V. Boyko, A. Pich, Y. Lu, S. Richter, K. -F. Arndt, H. -J. P. Adler, *Polymer*, 2003, **44**, 7821.
[46] C. Y. Loo, P. M. Young, W. H. Lee, R. Cavaliere, C. B. Whitchurch, R. Rohanizadeh, *Acta Biomater.*, 2012, **8**, 1881.
[47] X. P Xu, S. Chen, W. Tang, Y. J. Qu, X. Wang, *Polym. Eng. Sci.*, 2013, **98**, 659.
[48] Y. Haba, Y. S. Balazs, O. Carmiel, I. Katz, M. Narkis and A. Schmidt, *Polym. Adv. Technol.*, 2007, **18**, 756.
[49] M. Abbasian and A. A. Entezami, Polym. *Adv. Technol.*, 2007, **18**, 306.
[50] N. Moszner, U. Salz, and V. Rheinberger, *Polym. Bull.*, 1994, **32**, 411.
[51] T. Ribaut, P. Lacroix-Desmazes, B. Fournel, S. Sarrade, *J. Polym. Sci., Part A: Polym. Chem.*, 2009, **47**, 5448.
[52] Z. S. Hu, D. J. E. Ramírez, B. E. H. Cervera, G. Oskam, and P. C. Searson, *J. Phys. Chem. B*, 2005, **109**, 11209.
[53] M. S. Tokumoto, S. H. Pulcinelli, C. V. Santilli, and V. Briois, *J. Phys. Chem. B*, 2003, **107**, 568.
[54] M. S. Tokumoto, V. Briois, C. V. Santilli and S. H. Pulcinelli, *J. Sol-Gel Sci. Technol.*, 2003, **26**, 547.
[55] H. M. Xiong, X. Zhao, and J. S. Chen, *J. Phys. Chem. B*, 2001, **105**, 10169.
[56] L. Spanhel and M. A. Anderson, *J. Am. Chem. Soc.*, 1991, **113**, 2826
[57] Q. Zhang, S. J. Liu and S. H. Yu, *J. Mater. Chem.*, 2009, **19**, 191.
[58] J. A. Reyes-Labarta, A. Marcilla, *J. Appl. Polym. Sci.*, 2008, **107**, 339.
[59] Y. P. Mao, R. R. Qi, *J. Appl. Polym. Sci.*, 2008, **109**, 3249.
[60] D. Høvik, N. Hydro, *Thermochim. Acta*, 1985, **95**, 319.
[61] K. R. Carter, R. A. DiPietro, M. I. Sanchez, T. P. Russell, P. Lakshmanan and J. E. McGrath, *Chem. Mater.*, 1997, **9**, 105.
[62] S. W. Lei, Q. G. Guo, J. L. Shi, L. Liu, *Carbon*, 2010, **48**, 2644.
[63] S. W. Lei, Q. G. Guo, D. Q. Zhang, J. L. Shi, L. Liu, X. H. Wei, *J. Appl. Polym. Sci.*, 2010, **117**, 3545.
[64] W. M. Rohsenow, J. P. Hartnett, E. N. Ganic, *Handbook of Heat Transfer Fundamentals (2nd edition)*, New York: McGraw Hill, 1985: 236.

ToC graphic

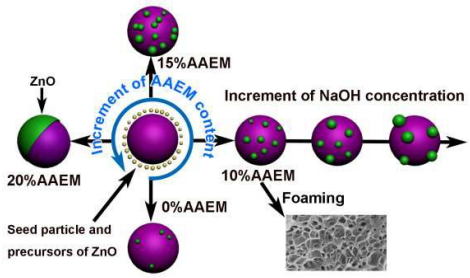

P(VC-co-AAEM)/ZnO nanoparticles are prepared by nano-coating method, and the morphology of raspberry-like particles is adjusted by hydrophilicity and NaOH concentration.